AlO_x Coating of Ultrastable Zeolite Y: A Possible Method for Vanadium Passivation of FCC Catalysts

Gabriela Catana,[†,⊥] Wolfgang Grünert,[‡] Pascal Van Der Voort,[§] Etienne F. Vansant,[§] Robert A. Schoonheydt,[†] and Bert M. Weckhuysen*,[†]

Centrum voor Oppervlaktechemie en Katalyse, Departement Interfasechemie, K. U. Leuven, Kardinaal Mercierlaan 92, B-3001 Heverlee, Belgium, Lehrstuhl für Technische Chemie, Rühr-Universität Bochum, D-44780 Bochum, Germany, and Laboratorium voor Anorganische Scheikunde, Departement Scheikunde, U. I. Antwerpen, Universiteitsplein 1, B-2610 Wilrijk, Belgium

Received: March 17, 2000

AlO_x coating is proposed as a possible method for vanadium passivation of the ultrastable zeolite Y (USY). Two coating methods are discussed: (i) the deposition of the $[Al_{13}O_4(OH)_{24}(H_2O)_{12}]^{7+}$ ($[Al_{13}]$) complex from aqueous solutions and (ii) the anchoring of alumoxane by in situ triisobutylaluminum hydrolysis followed by calcination. The properties and the efficiency in vanadium passivation of the coated materials have been investigated with DRS, ESR, XPS, FTIR, and sorption measurements. XPS revealed for all the coated samples an enrichment in the Al content in the near-surface region and differences in Al coordination geometry. Vanadyl(IV) etioporphyrin, the major contaminant in crude oil, was used to probe the trapping efficiency of the external AlO_x layer. The $[Al_{13}]$-derived layer is homogeneously distributed and covers the external surface of the USY zeolite, following its topology, but without blocking its pores. About 80% of the offered vanadyl species have been preferentially trapped in this layer. The alumoxane-based method is less efficient in vanadium passivation, most probably because after calcination the aluminum species are heterogeneously distributed, both on the external surface and in the channels of USY zeolite.

Introduction

Ultrastable zeolite Y (USY) is used as a catalyst in the fluid catalytic cracking (FCC) process, and its catalytic performances are seriously affected by metal contaminants such as vanadium or nickel present in crude oil as organic complexes.[1] These organic species, mostly porphyrins,[2−4] are deposited on the catalyst surface where they promote undesirable dehydrogenation reactions, which increase coke production at the expense of the gasoline yield. Moreover, vanadium reduces the overall catalyst activity and selectivity by destroying the zeolite crystallinity.[5]

In a previous paper, we reported on the preferential adsorption of vanadium ions on SiO_2, Al_2O_3, and USY.[6] Using a combination of diffuse reflectance spectroscopy and electron spin resonance, we found that both V^{4+} and V^{5+} were preferentially adsorbed on Al_2O_3, while they showed a much smaller preference for USY and SiO_2. This preference of $V^{4+/5+}$ species for alumina suggested to us a method to coat the external surface of USY with an AlO_x layer in order to prevent the poisoning of the catalyst with vanadium. The efficiency of the proposed method, based on the deposition of USY with the so-called Keggin ion, $[Al_{13}O_4(OH)_{24}(H_2O)_{12}]^{7+}$, was only indirectly proven via electron spin resonance of the vanadium impregnated materials.[6] A more detailed characterization of the Al species deposited on the external surface of the zeolite is obviously necessary.

Therefore, this paper gives a detailed account on the characterization of AlO_x-coated zeolites. Two coating methods are proposed, one based on the deposition of polymeric hydroxyaluminum complexes on USY and the other on alumoxane anchoring on the external surface of USY. The hydroxyaluminum polycations, $[Al_{13}O_4(OH)_{24}(H_2O)_{12}]^{7+}$, known as the Keggin ions, or $[Al_{13}]$ ions, are formed by partial hydrolysis of Al^{3+} in aqueous solutions and are deposited on the external surface of the zeolite, since their diameter is too big (9 Å) to enter the supercages of USY. Their structure is well-defined, with one tetrahedral Al surrounded by 12 octahedrally coordinated Al atoms.[7,8] Alumoxanes are oligomeric species with the general formula $[-Al(R)O-]_n$, obtained by the controlled hydrolysis of alkyl (R)-aluminum compounds.[9−12] If the water used in the hydrolysis process is coming from the hydrated zeolite, then the alumoxanes species can be directly anchored on the external surface of the zeolite. After calcination, the organic part is removed, obtaining a local enrichment in the aluminum content.

The physicochemical properties and the efficiency in vanadium passivation of the AlO_x-coated materials are investigated and compared. The techniques employed are X-ray photoelectron spectroscopy (XPS), X-ray diffraction (XRD), in situ Fourier transform infrared spectroscopy (FTIR), UV−vis−near-IR diffuse reflectance spectroscopy (DRS), electron spin resonance (ESR), and N_2 adsorption at 77 K.

Experimental Section

The following supports were used in this study: USY (CBV720, PQ Corporation) with a Si:Al ratio of 60, Al_{13}-coated USY (see further), alumoxane-coated USY (see further), and Al_2O_3 (Merck). Vanadium-loaded samples were prepared by the

* To whom correspondence should be addressed. E-mail: bert.weckhuysen@agr.kuleuven.ac.be.
[†] K. U. Leuven.
[‡] Rühr-Universität Bochum.
[§] U. I. Antwerpen.
[⊥] On leave from the National Institute of Materials Physics, Bucharest-Magurele, Romania.

10.1021/jp001021i CCC: $19.00
Published on Web 09/09/2000

incipient wetness technique with aqueous solutions of vanadyl sulfate ($VOSO_4 \cdot H_2O$, 96%, Janssen Chimica) or by contacting the samples with solutions of vanadyl(IV) etioporphyrin (VO-ETP, *pro analyse*, Strem Chemicals) in dichloromethane, to obtain a final vanadium loading of 0.1 wt %. In the latter case, the solvent was removed in vacuo using a rotary evaporator.

1. Preparation of the Keggin Ion Solutions and [Al_{13}] Coating of USY. The [Al_{13}] solutions were prepared according to the method of Furrer et al.[8] Two hundred fifty milliliters of a 0.25 M $AlCl_3$ solution (*pro analyse*, UCB) was heated in a water bath to 80 °C. Then, 600 mL of a 0.25 M NaOH solution (99%, Janssen Chimica) was added at a rate of 4 mL/min, while stirring at 300 rpm. After cooling this solution, 625 mL 0.1 M Na_2SO_4 (99%, UCB) was added, and during continuous stirring at 830 rpm a precipitate was formed over a 2 day period. This precipitate, $[Al_{13}O_4(OH)_{24}(H_2O)_{12}][(SO_4)_{7/2}]$, was filtered off, washed with distilled water, and freeze-dried. The obtained precipitate was redissolved with $Ba(NO_3)_2$ (*pro analyse*, Merck) in 1200 mL of H_2O in an ultrasonic bath for 4 h. The solution was separated from the precipitated $BaSO_4$ by filtration (0.1 μm, Millipore) and centrifugation at 11 000 rpm for 15 min.

[Al_{13}]-coated USY zeolite was obtained by mixing 1 g of USY zeolite in a 600 mL solution of [Al_{13}] at room temperature for 24 h. The solid product was separated by centrifugation, followed by washing and drying. The dried material was calcined overnight in air at 500 °C. This material is denoted as [Al_{13}]−USY. Successive depositions with [Al_{13}] resulted in [Al_{13}]-enriched USY materials, denoted as $[Al_{13}]_x$−USY (with x the number of depositions). The obtained materials were calcined overnight in air at 500 °C after each coating step.

2. Alumoxane Anchoring by in Situ Triisobutylaluminum Hydrolysis. One gram of USY zeolite was equilibrated against a relative humidity of 79.5% (in a desiccator over a NH_4Cl saturated aqueous solution) at room temperature, corresponding to 20 wt % sorbed water. The water-saturated sample was suspended in 20 mL of toluene in a reaction vessel, which was flushed with nitrogen and cooled to 273 K (ice bath) under continuous stirring. A 1 M solution of triisobutylaluminum (*pro analyse*, Aldrich) in toluene was added slowly to the suspension, in order to have a molar ratio $H_2O/(i\text{-Bu})_3Al$ of 0.5, 1, 1.5, 2, and 3. After warming the mixture under stirring to room temperature, the solid product was recovered by centrifugation (10 000 rpm), washed with toluene, and finally dried in air at 333 K. The dried materials were calcined overnight, in air, at 823 K, and the resulted samples were labeled as $[BAO]_y$−USY, where y is the molar ratio $H_2O/(i\text{-Bu})_3Al$.

3. Pretreatment and Experimental Techniques. In situ FTIR spectra were recorded in the region 4000−1000 cm^{-1} on a Nicolet 730 spectrometer, equipped with a DTGS (deuterated triglycine sulfate) detector, with a resolution of 2 cm^{-1}, using a homemade cell and thin self-supported wafers (8−10 mg/cm^2). The cell was connected to an evacuation-gas flow system, which allowed treatments up to 500 °C when the CaF_2 windows were cooled with circulating tap water.

Surface areas and pore volumes were determined at 77 K using nitrogen adsorption, on a Coulter Omnisorp 100 apparatus. The samples were first evacuated overnight at 250 °C. The data were interpreted using the BET (Brunauer, Emmett, and Teller) theory for the surface areas and the *t*-plot method for the pore volumes.

X-ray powder diffractograms were obtained using a Siemens D5000 X-ray diffractometer with Cu Kα radiation.

Liquid ^{27}Al NMR measurements were performed with a Bruker AMX 300 spectrometer at 78.208 MHz, with a pulse length of 6 μs and a pulse delay of 5 s. A 0.25 M $Al(OH)_4^-$ solution in D_2O was used as a reference, since it presents a single resonance at 80 ppm.

TABLE 1: Surface Areas and Pore Volumes of the AlO_x-Coated Samples and Their Relative Decrease in Comparison with the Surface Area (S_0) and the Pore Volume (V_{p0}) of the Parent Zeolite

sample	S_{BET} (m^2/g)	S/S_0 (%)	V_p (ml/g)	V_p/V_{p0} (%)
USY	599.0		0.226	
$[Al_{13}]_1$−USY	544.4	90	0.225	99
$[Al_{13}]_2$−USY	526.2	87	0.215	95
$[Al_{13}]_3$−USY	519.1	86	0.211	93
$[BAO]_{0.5}$−USY	503.2	84	0.201	88
$[BAO]_1$−USY	460.9	76	0.182	80
$[BAO]_2$−USY	398.8	66	0.154	68

Diffuse reflectance spectra were taken with a Varian Cary 5 UV−vis−near-IR spectrometer at room temperature. The samples were granulated, and the size fraction 0.25−0.4 mm was loaded in a quartz cell with Suprasil window. The spectra were recorded against a halon white reflectance standard in the range 200−2500 nm. The computer processing of the spectra consisted of the following steps: (1) subtraction of the baseline, (2) conversion to wavenumber, and (3) calculation of the Kubelka−Munk (K−M) function.

ESR spectra were taken with a Bruker ESP300E spectrometer in X-band (9.5 GHz) with a double rectangular TE_{104} mode cavity. The modulation frequency and amplitude were 100 kHz and 5 G, respectively.

XPS measurements were performed with a Leybold LHS 10 MCD spectrometer (base pressure $< 10^{-9}$ mbar). XP spectra were excited with Mg Kα irradiation (1253.6 eV, operated at 10 kV and 22 mA), and the Al(2p), O(1s), and Si(2p) lines were recorded. In addition, the Al KLL Auger line was measured as excited by the bremsstrahlung. The samples, which had been stored in ambient atmosphere, were deposited on the sample holder from a slurry in *n*-pentane and transferred into the ultrahigh vacuum by standard procedures without any previous treatment. The referencing of the binding-energy (BE) scale will be discussed under Results and Discussion.

Results and Discussion

1. [Al_{13}] Deposition of Ultrastable Zeolite Y. The ^{27}Al NMR spectrum of the [Al_{13}] aqueous solution shows only one peak at 62.5 ppm, corresponding to the central, tetrahedrally coordinated Al^{3+}, which confirms the presence and stability of the [Al_{13}] ion.[8] In our previous study[6] we reported that the amount of [Al_{13}] taken up by the zeolite material increases with the offered amount of [Al_{13}], but levels off at 0.11 mmol of Al/g of USY for a concentration of the initial solution equivalent with 20 mmol of Al/g of USY. To have higher amounts of aluminum fixed on the zeolite, the [Al_{13}]−USY material was first calcined at 500 °C and then contacted again with the Keggin ion solution. This procedure was repeated up to three times. The ^{27}Al NMR spectrum of the [Al_{13}] solution after contacting it with the zeolite presents also only one peak at 62.5 ppm. This is an indication that during the deposition procedure the Keggin complex was not fragmented and no other species were formed in the solution.

The XRD patterns of $[Al_{13}]_x$−USY materials were very similar to those of the pure USY material, although for the highest [Al_{13}] loading some amorphous background could be observed. The BET surface area decreases slightly with the number of [Al_{13}] depositions, as presented in Table 1. The pore volumes of the coated samples remain almost unchanged, except

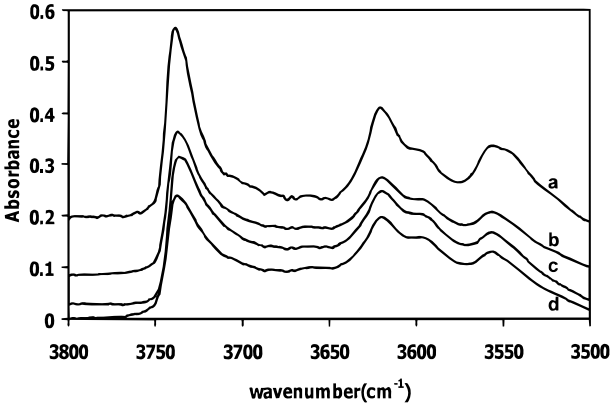

Figure 1. IR spectra in the hydroxyl stretching region of USY and $[Al_{13}]_x$−USY samples, after calcination and dehydration (500 °C, evacuation at 0.1 mbar): (a) USY, (b) $x = 1$, (c) $x = 2$, and (d) $x = 3$.

for the highest loading ($x = 3$) when a slight decrease is observed. It is worthwhile to notice that, when compared with the parent zeolite, the relative decrease of the pore volumes (V_p/V_{p0}) is lower than the relative decrease of the surface area (S/S_0) for all the $[Al_{13}]$ coated samples. This suggests that the zeolite pores remain accessible after the coating procedure and that only a partial blocking of the zeolite channels could take place for the highest $[Al_{13}]$ loading.

The IR spectra in the OH stretching region of the $[Al_{13}]$-deposited samples, $[Al_{13}]_x$−USY, are shown in Figure 1. They were recorded for the calcined samples after dehydration in a vacuum at 500 °C. To compare the spectra quantitatively, the intensities of the IR absorption peaks were normalized to the wafer density. A decrease of the 3740 cm^{-1} band attributed to free silanols is observed for all the coated samples. As a consequence, the anchoring mechanism involves most probably a proton exchange reaction as well as an interaction of Al_{13}^{7+} with hydroxyl groups. At the same time, with the increasing number of depositions we notice an increase of the band at 3600 cm^{-1}, characteristic of extraframework aluminum species. For all the coated zeolites, the IR spectra still show the 3620 and 3560 cm^{-1} maxima, characteristic of the acidic OH groups in the supercages and, respectively, in the sodalitic cages. This means that the $[Al_{13}]$-coating procedure is not altering the acid properties of the catalyst. In other words, as long as the pores are still accessible, there are acidic sites available for catalytic action.

Table 2 summarizes the XPS binding energies, Al KLL kinetic Auger energies (KE), line widths (fwhm, full width at half-maximum), and elemental ratios in the XPS sampling region for the $[Al_{13}]_x$−USY. The corresponding Auger lines are shown in Figure 2a. In addition, the modified Auger parameters α'_{Al} (α'_{Al} = BE(Al(2p)) + KE(Al KLL)) are reported. Except for the initial USY and the Al Auger lines, all signals have an almost symmetrical shape. Although intact zeolites usually exhibit symmetric lines, a slight asymmetry of the signal shapes as observed with USY is within expectation for a highly dealuminated sample, in which all elements may occur in different environments. Since the overall line widths (2.3−2.6 eV) were not unexpectedly high, no attempt was made to analyze the asymmetries. Any additional state responsible for them should have a binding energy close to the peak maximum. On the other hand, the Al KLL Auger line of USY was both asymmetric and broadened and could be fitted by two components that provided Auger parameters of 1458.7 and 1461.5 eV together with the BE at the Al(2p) peak maximum. The Auger lines of the coated samples were more symmetric, but exhibited a minor feature at low kinetic energy yielding an Auger parameter of 1454.5−1455 eV.

In Table 2, binding energies are given as referenced to C(1s) = 284.5 eV, and to Si(2p) = 103.0 eV (in italics). With the C(1s) reference, there is large scatter in the Si(2p) binding energies, which is, certainly, unrealistic since most of the silicon should not be strongly affected by the Al deposition (see also below). Moreover, for the dealuminated USY, the BE values of the framework elements are even lower than values reported earlier for the zeolite Y with normal Al content (O(1s) = 531.8−532.0 eV, Si(2p) = 102.4−102.6 eV), and it is known that these binding energies increase with decreasing Al content owing to Madelung effects.[13] Due to these obvious problems with the carbon reference in our samples, silicon was employed as a secondary reference setting Si(2p) to a value as found with high-silica zeolites, e.g., ZSM-5 (103.0 ± 0.1 eV [13]). With this calibration, the O(1s) and Al(2p) binding energies of USY also shifted into the ranges typical of this zeolite composition.[13]

Recent studies[14] have shown that the Al Auger parameter may be used to discriminate Al in different coordination states. According to ref 14, the Al species detected in our USY may be attributed to tricoordinated Al (Lewis site, ca. 1458 eV) and octahedral, i.e., extralattice Al (>1461 eV). This does not necessarily mean that there is no tetracoordinated Al in our sample, since a third component with an intermediate Auger parameter (1460−1460.5 eV) could be identified from the measured signal only if present with considerable weight. However, together with the elemental ratios reported in Table 2, the failure to detect tetrahedral Al implies, indeed, that it is a minority species in the near-surface region. The Si/Al ratio is significantly lower than the bulk value (60), most likely due to extraframework Al.

With $[Al_{13}]$ deposited, all lines (including Si(2p)) become broader, but there is an extra broadening for O(1s) and Al(2p). For the latter, the broadening may be ascribed to a difference in binding energy between the atoms in the zeolite and in the $[Al_{13}]$-derived material. This is most obvious with aluminum, for which the species in the overlayer becomes the majority species with increasing number of depositions, which results in a binding-energy shift. The same is true for the Auger parameter. With oxygen, there is always a large contribution from zeolite O, hence the binding energy is not changed. The broadening of the Si(2p) line may indicate that the Si in the external zeolite layer is changed by the coating process (e.g., formation of Si−O−Al linkages; see IR results), which would result in an additional Si component with a modified binding energy. Since the effect results only in a line broadening and not in a shoulder or a new signal, the BE differences involved are minor and should not significantly affect the BE scale referenced to the Si(2p) signal.

Both the Al(2p) BE of the $[Al_{13}]$-derived layer (extrapolated 75.1−75.2 eV) and the Auger parameter (extrapolated 1460.5−1460.6 eV) are definitely different from what is known for different forms of Al_2O_3 (73.6−74.0 eV, Auger parameter 1461.5−1462.0 eV [15]). This is highly significant for just the Auger parameter since it is not subject to the referencing problem of the binding-energy scale. Although an Al(2p) BE of 75 eV is rare with Al compounds, it is, however, near the range found with tetrahedrally coordinated Al in H zeolites (74.7−74.9 eV [13]). The Auger parameter of 1460.5 eV is in the range ascribed to tetrahedrally coordinated Al.[14] The significance of the minor Auger signal is not known. The Al KLL transition has three components (KL_3L_3, KL_2L_3, and KL_2L_2), which should

TABLE 2: Binding Energies, Kinetic Auger Energies, and Auger Parameters of [Al_{13}]-Coated and Alumoxane-Coated USY[a]

sample	Si(2p) BE (fwhm)		O(1s) BE (fwhm)		Al(2p) BE (fwhm)		Al KLL	α'_{Al}	Si/Al	Si/O	t	t^b (nm)
(a) [Al_{13}]-Coated USY												
USY	101.6 (2.6)	*103.0* (asym)	531.1 (2.6)	*532.5* (asym)	73.1 (2.3)	*74.5* (asym)	*1384.2* (*1387.0*)[c]	1458.7 (1461.5)[c]	19.5	0.50		
[Al_{13}]$_1$−USY	102.2	*103.0* (3.0)	531.6	*532.4* (3.1)	74.1	*74.9* (3.1)	*1385.0*	1459.9	6.3	0.45	0.07λ	0.28
[Al_{13}]$_2$−USY	102.3	*103.0* (2.9)	531.7	*532.4* (3.1)	74.3	*75.0* (3.0)	*1385.2*	1460.2	4.5	0.43	0.11λ	0.44
[Al_{13}]$_3$−USY	101.8	*103.0* (3.0)	531.2	*532.4* (3.1)	73.9	*75.1* (3.1)	*1385.3*	1460.4	4.1	0.42	0.12λ	0.5
(b) Alumoxane-Coated USY												
[BAO]$_{0.5}$−USY	103.0	*103.0* (2.6)	532.5	*532.5* (3.0)	74.8	*74.8* (2.7)	*1385.7*	1460.6	3.15	0.39	0.25λ	1.0
[BAO]$_1$−USY	102.7	*103.0* (2.6)	532.1	*532.4* (3.3)	74.4	*74.7* (2.7)	*1386.1*	1460.8	1.37	0.29	0.53λ	2.1
[BAO]$_2$−USY	102.6	*103.0* (2.7)	531.9	*532.3* (3.5)	74.3	*74.7* (2.7)	*1386.4*	1461.1	0.39	0.23	1.26λ	5
[BAO]$_3$−USY	102.4	*103.0* (2.8)	531.7	*532.3* (3.6)	74.1	*74.7* (2.8)	*1386.3*	1461.0	0.48	0.16	1.12λ	4.5

[a] All energies (including half-widths, fwhm) are in eV; calibration: C 1s = 284.5 eV; *Si 2p = 103.0 eV*, (*italics*). [b] With λ = 4 nm; see text. [c] Minor component.

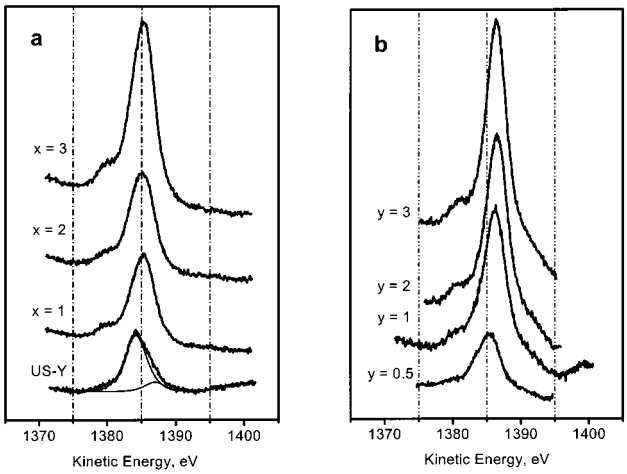

Figure 2. Al KLL Auger spectra of USY and the AlO_x-coated USY: (a) parent sample, USY, and [Al_{13}]$_x$−USY samples, x = 1, 2, 3; (b) alumoxane-coated samples, [BAO]$_y$−USY, y = 0.5, 1, 2, 3.

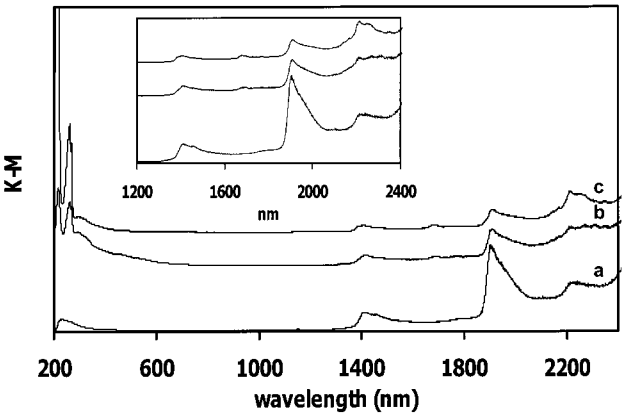

Figure 3. DRS spectra (1200−2400 nm) of USY and [BAO]$_y$−USY samples: (a) USY, (b) y = 1, and (c) y = 3.

be, however, too close to each other to be resolved in our samples. An Auger parameter as calculated for the minor signal (1454.5−1455 eV) has not been reported in the literature to our knowledge.

As expected, both the Si/Al ratio and the Si/O ratio decrease with increasing [Al_{13}] deposition. Table 2 contains results of calculations performed to estimate the average thickness of the AlO_x layer on the zeolite surface from the Si/Al ratios measured. For this purpose, the Al density in the overlayer was assumed to be equal to the Si density in the zeolite. With this model, the layer thickness (t) produced was estimated to be 7−12% of the mean free photoelectron path λ of the Si(2p) or Al(2p) photoelectrons in the overlayer. The latter parameter was estimated for γ-Al_2O_3 from a correlation by Seah and Dench[16] to be 1.87 nm; for a structure of a porosity comparable with that of a zeolite this has to be multiplied by 2−2.5 (i.e., ≈4 nm). The layer thickness achieved with the [Al_{13}]-deposition method should be, therefore, around 3−5 Å.

2. Alumoxane Anchoring by in Situ Triisobutylaluminum Hydrolysis. It is known from the literature that the hydrolysis of triisobutylaluminum proceeds in several steps, and is a function of the H_2O/Al molar ratio.[11,12] If H_2O/Al is less than or equal to 1, a complex of (i-Bu)$_3$Al with H_2O is first formed. This complex undergoes intramolecular rearrangement to give diisobutylaluminum hydroxide, (i-Bu)$_2$AlOH, and forms stable autoassociates or reacts with the excess (i-Bu)$_3$Al to give alumoxanes. The formation of dialkylaluminum hydroxide is the dominating reaction until the water is used up. For hydrolysis ratios greater than 1, aluminum hydroxides are formed altogether with the bulky alumoxane structures, while for H_2O/Al greater than 3, the aluminum hydroxide species are preferentially and rapidly formed.

In this work, the water used in the hydrolysis process is coming from the hydrated zeolite, resulting in the formation of alumoxane species at the external surface of the zeolite. It is then clear that the molar ratio H_2O/(i-Bu)$_3$Al will have an effect on the characteristics of the aluminum oxide coating obtained.

In a first step, we studied the alumoxane anchoring by diffuse reflectance spectroscopy. Figure 3 shows the DRS spectra of the alumoxane-coated samples, [BAO]$_y$−USY, with different values of the H_2O/Al ratio. The UV region of the coated samples presents several absorption bands assigned to the solvent (toluene) and a broad, less intense, band around 300 nm due to an oxygen to aluminum p_π−d_π dative bond, typical for the oxygen-bridged organoaluminum compounds.[17,18] In the near-IR region (see the insert, Figure 3), the samples are characterized by several absorption bands: the band at 1410 nm could be assigned to the overtone of the stretching mode of the silanol groups, while the band at 1458 nm could be assigned to the overtone of the OH stretching in water molecules. Both of them are decreasing during triisobutylaluminum hydrolysis. The new

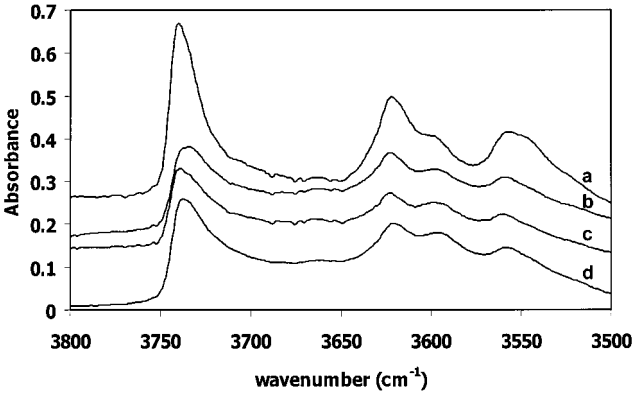

Figure 4. IR spectra in the hydroxyl stretching region of USY and $[BAO]_y$−USY samples, after calcination and dehydration (500 °C, evacuation at 0.1 mbar): (a) USY, (b) $y = 3$, (c) $y = 1$, and (d) $y = 0.5$.

shoulder which appears at 1383 nm for the coated samples (b and c) could be assigned to OH groups of the alumoxane structure or of the intermediate hydroxide formed. Moreover, one can notice that the higher the H_2O/Al ratio, the more pronounced is this shoulder.

The $(\nu + \delta)$ combination band of OH in water molecules appears at 1910 nm and that of structural OH appears at 2200−2400 nm, depending on the environment. Both of them are decreasing for the coated samples. The water is consumed during the triisobutylaluminum hydrolysis, but it is again present in the coated samples stored in air, and therefore no clear statements can be made based only upon the variation of these peaks. For the coated samples, CH stretching overtones appear at 1675 and 1690 nm and the CH combination mode is present at 2300 nm. A shoulder appears at 2250 nm in the spectra of the modified samples. This absorption was previously assigned by several authors[19−21] to bridging OH, of the type Al−OH−Al, or between three Al, environments characteristic in our case to the alumoxane coating.

In a next step, we have determined the pore volume and surface area of the calcined samples as a function of the H_2O/$(i\text{-Bu})_3Al$ ratio, y. The results of the surface area and pore volume measurements are summarized in Table 1. One can notice a decrease both in the surface area and in the pore volume, higher than that observed in the case of the $[Al_{13}]$-deposited samples. The relative decrease of the pore volumes (V_p/V_{p0}) is—for all the alumoxane-coated samples—of the same magnitude as the relative decrease of the surface area (S/S_0). Thus, the coating procedure is most probably inducing a pore-narrowing effect. The alumoxane species initially formed are anchored on the external surface via the silanol groups, but they are fragmented and migrate into the pores during the calcination step. The decrease in the surface area and the pore volume is related to the hydrolysis mechanism, namely the higher the hydrolysis ratio used, the lower the surface area and the pore volume obtained. For instance, for a value of y equal to 3, aluminum hydroxide species are formed and they could easily migrate into the pores. In addition, the crystallinity of the alumoxane-coated samples was verified by XRD. In all cases the sample remained highly crystalline, although a small amorphous background could be observed for the highest hydrolysis ratio employed.

Figure 4 presents the IR spectra in the OH stretching region of the coated $[BAO]_y$−USY samples. They were recorded after dehydration at 500 °C and subsequent evacuation. Comparing the spectra of the coated samples with the spectrum of the parent zeolite (USY) indicates a decrease of the band from 3740 cm^{-1}, attributed to free silanols. This suggests that the anchoring mechanism of the alumoxane species proceeds via external OH groups, which serve as docking points for the deposited layer. The intensities of the bands assigned to the acidic OH groups (at 3620 and 3560 cm^{-1}) decrease especially for the highest hydrolysis ratios, when the aluminum species formed are small enough to enter the pores. At the same time, the band characteristic to extraframework aluminum, at 3600 cm^{-1}, is slightly increasing. Thus, the alumoxane-coating procedure is leaving—especially at low hydrolysis ratios—enough acidic sites available for the catalytic process.

Table 2 shows XPS results obtained for the alumoxane-coated USY. Again, the binding energies will be discussed as referenced to Si(2p) = 103.0 eV. There are significant differences when compared to the $[Al_{13}]$-coated materials. Most obvious is the larger thickness of the alumoxane-derived layers. In all cases, the Si/Al ratio is below the values measured after the deposition with the Al polyanions. In the samples with higher deposited Al content, the layer thickness is on the order of the photoelectron escape depth, i.e., several nanometers.

While the O(1s) binding energy does not depend on the type of AlO_x coating, the Al(2p) BE is somewhat smaller with the alumoxane-derived material. More significantly, due to higher kinetic Auger energies, its Al Auger parameter is significantly higher than that of the $[Al_{13}]$-derived coating. The Auger parameter of ≥ 1461 eV suggests a predominantly octahedral coordination in the alumoxane-derived material, but there is still a significant difference from aluminas (α or γ), which exhibit lower Al(2p) binding energies and higher Auger parameters (vide supra).

There are also significant differences in line width trends with the different AlO_x-coated surfaces. With the alumoxane-derived material, the trends for Al(2p) and O(1s) are determined by the overlayer. This is the case for Al(2p) since the Al atoms are located in the coating, and for O(1s) because there is neither a binding-energy shift nor a line asymmetry although the overlayer oxygen may contribute up to two-thirds of the oxygen detected by XPS (cf. Si/O ratios in Table 2). Remarkably, the line widths are smaller than in the $[Al_{13}]$-coated material with Al(2p), but larger with O(1s). It appears that the electronic and coordination properties of Al differ less in the thick alumoxane-derived layer than in the thin $[Al_{13}]$ coating, and the opposite applies for the oxygen, which may coexist in OH groups and Al−O−Al bridges. Remarkably, there are also differences in the line width trends of Si, which belongs totally to the zeolite: the width of the Si(2p) line is smaller in the alumoxane-coated samples and remains near the value for USY. The properties of the Si atoms seen by XPS in these materials seem to exhibit less variation than in the $[Al_{13}]$-coated ones, where the Si line broadening had been interpreted as an indirect indication for the condensation of external silanol groups with the AlO_x coating. The conclusion that such condensation is not taking place in the alumoxane-coated material has to be rejected on the basis of the IR spectra discussed above (Figure 4). Instead, the Si(2p) line width trend supports another conclusion of this study, the mobility of AlO_x species in the alumoxane preparation and their diffusion into the pores of the external zeolite layer. By involving siloxane groups at lattice defects, which should be abundant in USY, into condensation reactions, they might convert much of the Si content of the external crystallite region into a state which is present only at the outermost surface in the $[Al_{13}]$ preparation. This would explain the more narrow

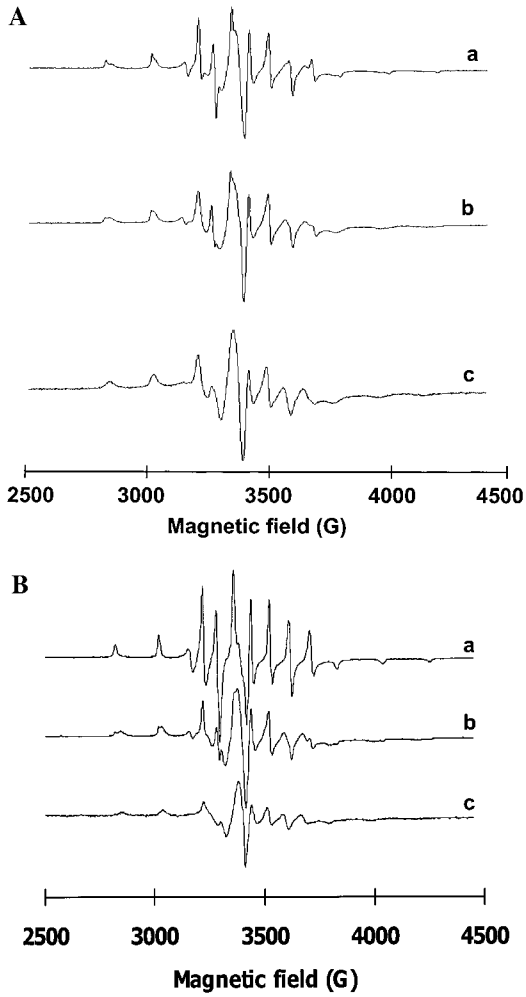

Figure 5. ESR spectra of $VOSO_4$-impregnated samples (0.1 wt % V): (A) $[Al_{13}]_x$−USY samples: (a) $x = 1$, (b) $x = 2$, and (c) $x = 3$; (B) USY and $[BAO]_y$−USY samples: (a) USY, (b) $y = 0.5$, and (c) $y = 3$.

distribution of the properties of Si sites in the alumoxane-derived materials and, consequently, the lower Si(2p) line widths in these materials.

3. Vanadium Passivation. In a previous paper[6] we have studied the preferential adsorption and mobility of vanadium species on different oxidic supports. We found that both V^{4+} and V^{5+} ions show the following preference order: $Al_2O_3 > SiO_2 \geq$ USY. This could be interpreted in relation with a stable coordination geometry formed when an oxide ligand of Al_2O_3 is directly coordinated to VO^{2+} along the axial position. The same preference sequence was observed for Cr^{n+} ions.[22]

To verify the efficiency in vanadium trapping of the coated materials, we recorded the ESR spectra of vanadyl sulfate impregnated samples. Figure 5 shows the ESR spectra of the $[Al_{13}]_x$−USY samples as a function of the number of depositions with $[Al_{13}]$, x (A), and of the $[BAO]_y$−USY samples as a function of the hydrolysis ratio, y (B). Such ESR spectra are typical for V^{4+}, with a d^1 configuration and a nuclear spin I of $^7/_2$. The experimental spectra consist each of two signals assigned to V^{4+}on USY and, respectively, V^{4+} on alumina. The corresponding ESR parameters and weight coefficients of the component signals were obtained as follows: (1) separate simulation[23] of the ESR spectra of V^{4+}/USY (S_z) and V^{4+}/Al_2O_3 (S_a) (the g- and A-values obtained are listed in Table 3); (2) summation of both spectra with appropriate weight coefficients ($S = c_zS_z + c_aS_a$); (3) comparison of the simulated spectrum (S) with the experimental one, followed by possible reevaluation of the coefficients and reiteration.

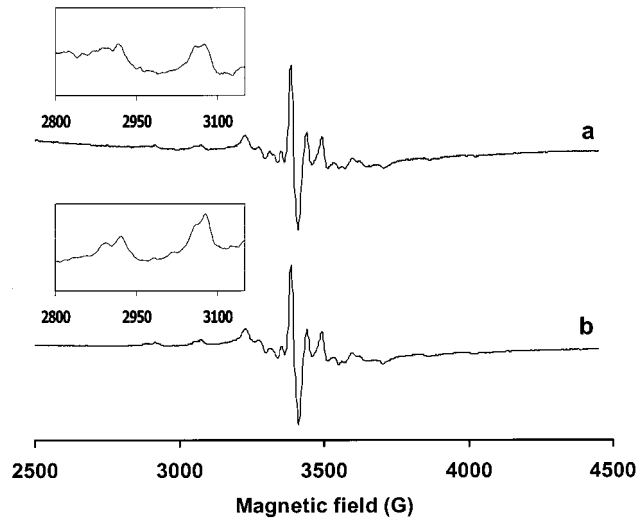

Figure 6. ESR spectra of VOETP-loaded samples (0.1 wt % V): (a) $[BAO]_1$−USY, (b) $[Al_{13}]_3$−USY. The (2800−3150) Gauss region is expanded in the insert.

The obtained values of c_z and c_a for different AlO_x-coated materials are summarized in Table 4. These values clearly indicate the preferential adsorption of V^{4+} on the alumina-like phase of the coated samples. The c_a coefficient increases with the amount of aluminum deposited per gram of zeolite in both procedures. However, V^{4+} with an "alumina-like" environment can be localized on both the external and internal surfaces of the zeolite, since the impregnation with $VOSO_4$ makes these alumina-like phases equally reachable. Thus, the increase of the c_a coefficient is not necessarily a proof for the existence of a uniform external AlO_x layer, since it can be related as well with the increase in the extraframework Al deposits inside the zeolite cages.

Therefore, we have loaded the samples with vanadyl(IV) etioporphyrin (VOETP), an organic complex present in crude oil, which is too big to enter the zeolite pores. In this way, we can verify the efficiency in vanadium trapping of the AlO_x deposits at the external surface of USY. Figure 6 presents the ESR spectra of vanadyl(IV) etioporphyrin (0.1 wt % V) loaded on the AlO_x-coated samples. Two distinct signals were observed in all cases, but their relative weight in the total spectrum was different as a function of the support. It is clear that both signals are due to adsorbed VOETP species, coordinated to different sites on the surface of the investigated materials. We can assign one signal to the complex coordinated via V^{4+} to a Lewis basic

TABLE 3: ESR Parameters of the Signals Characteristic to $VOSO_4$- and VOETP-Loaded Al_2O_3 and USY

support	signal label	g_{xx}	g_{yy}	g_{zz}	A_{xx} (G)	A_{yy} (G)	A_{zz} (G)
$VOSO_4/Al_2O_3$	a	1.985	1.983	1.947	84.9	89.9	209.3
$VOSO_4$/USY	z	1.984	1.981	1.936	77.1	72.8	197.2
VOETP/Al_2O_3,USY	1	1.985	1.981	1.968	58.9	58.9	167.9
	2	1.974	1.974	1.965	57.1	53.5	166.1

TABLE 4: Weight Coefficients (c_z and c_a) of the Simulated ESR Spectra of $VOSO_4$-Loaded Samples

$[Al_{13}]_x$−USY	c_z	c_a	$[BAO]_y$−USY	c_z	c_a
$x = 1$	0.65	0.35	$y = 0.5$	0.47	0.53
$x = 2$	0.45	0.55	$y = 1$	0.31	0.69
$x = 3$	0.15	0.85	$y = 3$	0.04	0.96

TABLE 5: Weight Coefficients (c_1 and c_2) of the Simulated ESR Spectra of VOETP-Loaded Samples

support	c_1	c_2
Al_2O_3	0.09	0.91
USY	0.89	0.11
$[Al_{13}]_3$−USY	0.20	0.80
$[BAO]_1$−USY	0.32	0.68

site (center type 1) and the other signal to the vanadyl group bonded through the oxygen onto an acceptor site (center type 2). A similar interpretation was proposed by Knözinger et al.[4] for vanadyl tetraphenylporphyrin loaded on alumina.

In our case, the signal corresponding to VOETP fixed on center 1 is more intense in the spectrum of USY, while its relative intensity on alumina is much smaller. By contrast, the signal corresponding to VOETP fixed on center 2 is predominant on alumina. VOETP loaded on the AlO_x-coated samples shows ESR spectra which are clearly composed of both signals (see inserts in Figure 6), with different weight coefficients, $S = c_1S_1 + c_2S_2$. These coefficients were determined by spectrum simulation,[23] starting with the separate simulation of the ESR signals 1 and 2, followed by summation of both signals and reevaluation of the coefficients until a good convergence was obtained between the simulated and the experimental spectra. The calculated coefficients are listed in Table 5. Thus, in the case of VOETP loaded on $[Al_{13}]_3$−USY sample, the signal corresponding to VOETP fixed on center 2 has a major contribution to the total spectrum (80%), while its contribution in the case of $[BAO]_1$−USY sample is less important (68%).

The coated samples are alumina rich in the near-surface region, and therefore an increased number of Lewis acid sites are available for the adsorbed VOETP. This explains the higher values of the c_2 coefficient for the coated samples in comparison with that for the parent zeolite (11%). Moreover, we can conclude that with the $[Al_{13}]$-deposition method an effective coating was achieved, although it is not a total coverage of the external surface of the zeolite. The results also show that the alumoxane coating method is less efficient in vanadium passivation, most probably because after calcination part of the aluminum species have migrated inside the zeolite channels, where they cannot act as traps for VOETP.

Conclusions

Two different AlO_x coating methods of USY zeolite have been evaluated in this study: (i) the deposition of the $[Al_{13}O_4(OH)_{24}(H_2O)_{12}]^{7+}$ complex from aqueous solutions and (ii) the anchoring of alumoxane by in situ triisobutylaluminum hydrolysis followed by calcination.

FTIR and liquid N_2 sorption measurements revealed that with the $[Al_{13}]$-deposition method the acidic properties of the parent zeolite are not dramatically altered and the zeolite pores are still accessible.

The alumoxane species formed by triisobutylaluminum hydrolysis and anchored onto the external surface of the zeolite were evidenced by DRS. After calcination only part of the alumoxane-derived species remains on the external surface, while an important fraction probably migrates into the zeolite pores. The decrease in the surface area and the pore volume for the alumoxane-coated USY is more pronounced than in the case of $[Al_{13}]$-deposited USY, and this is most probably due to a pore-narrowing effect. The acidic properties of the alumoxane-coated USY are slightly affected for the highest hydrolysis ratios.

The Si/Al and Si/O ratios of AlO_x-coated USY as determined by XPS show a remarkable decrease in the near-surface region, clearly indicating an enrichment in the Al content. The Al(2p) binding energies and the Al Auger parameters in the $[Al_{13}]$-deposited USY samples are in the range ascribed to tetrahedrally coordinated Al, while those for the alumoxane-derived USY material are typical for octahedrally coordinated Al. Moreover, the narrow distribution of the properties of Si sites in the alumoxane-coated USY supports the hypothesis of the migration of AlO_x species into the pores during the calcination step. The average thickness of the AlO_x layer on the zeolite was estimated to be around 3−5 Å in the case of $[Al_{13}]$-deposited samples and between 1 and 4.5 nm for the alumoxane-coated samples.

Vanadyl(IV) etioporphyrin, the major contaminant in crude oil, was used to probe the trapping efficiency of the external AlO_x layer. It has been shown that with the $[Al_{13}]$-deposition method 80% of the offered vanadyl species could be preferentially trapped. The alumoxane-based method is less efficient in vanadium passivation.

Therefore we conclude that with the $[Al_{13}]$ method an effective AlO_x coating was achieved: although thin, the $[Al_{13}]$-deposited layer is homogeneous and covers the external surface of USY zeolite following its topology, but without blocking its pores. By contrast, in the case of alumoxane-derived samples we can hardly speak of a layer. After calcination, the aluminum species are heterogeneously distributed, most probably fixed in small clusters both on the external surface and in the zeolite channels.

Acknowledgment. This work was supported in the framework of a cooperation program (BIL 96/22) between the Ministry of the Flemish Community (Belgium) and the Ministry of Research and Technology (Romania). B.M.W. and P.V.D.V. are postdoctoral fellows of the Fonds voor Wetenschappelijk Onderzoek-Vlaanderen (F.W.O.). The authors thank Prof. P. J. Grobet for the ^{27}Al NMR measurements and H. Leeman for technical assistance.

References and Notes

(1) Magee, J. S.; Mitchell, M. M. Jr. *Stud. Surf. Sci. Catal.* **1993**, *76*, 105.
(2) Mitchell, P. C. H.; Scott, C. E.; Bonnelle J. P.; Grimblot J. G. *J. Chem. Soc., Faraday Trans. 1* **1985**, *81*, 1047.
(3) Mitchell, P. C. H.; Scott, C. E. *Polyhedron* **1986**, *5*, 237.
(4) Knözinger, H.; Cordischi, D.; Vielhaber, B. *Catal. Today* **1990**, *7*, 447.
(5) Truhillo, C. A.; Uribe, U. N.; Knops-Gerrits, P. P.; Oviedo L. A.; Jacobs, P. A. *J. Catal.* **1997**, *168*, 1.
(6) Catana, G.; Rao, R.; Weckhuysen, B. M.; Van Der Voort, P.; Vansant, E. F.; Schoonheydt, R. A. *J. Phys. Chem. B* **1998**, *102*, 8005.
(7) Schoonheydt, R. A.; Leeman, H.; Scorpion, A.; Lenotte, I.; Grobet, P. *Clays Clay Miner.* **1994**, *42*, 518.
(8) Furrer, G.; Ludwig, C.; Schindler, P. W. *J. Colloid Interface Chem.* **1992**, *149*, 56.
(9) Tritto, I.; Sacchi, M. C.; Locatelli P. *Macromol. Chem. Phys.* **1996**, *197*, 1537.
(10) Mason, M. R.; Smith, J. M.; Bott, S. G.; Barron, A. R. *J. Am. Chem. Soc.* **1993**, *115*, 4971.
(11) Boleslawski, M.; Serwatowski, J. *J. Organomet. Chem.* **1983**, *255*, 269.
(12) Pasynkiewicz, S. *Polyhedron* **1990**, *9*, 429.
(13) Grünert, W.; Muhler, M.; Schröder, K.-P.; Sauer, J.; Schlögl, R. *J. Phys. Chem.* **1994**, *98*, 10920.
(14) Filippone, F.; Moretti, G. *Appl. Surf. Sci.* **1998**, *135*, 150.
(15) Wagner, C. D. In *Practical Surface Analysis*, 2nd ed.; Briggs, D., Seah, M. P., Eds.; Wiley: New York, 1990; Appendix 5.

(16) Seah, M. P.; Dench, W. A. *Surf. Interface Anal.* **1979**, *1*, 2.
(17) Giannetti, E.; Nicoletti, G. M.; Mazzocchi, R. *J. Polym. Sci.* **1985**, *23*, 2117.
(18) Van Looveren L. Ph.D. Thesis, K. U. Leuven, 1998.
(19) Vicente, M. A.; Lambert, J. F. *Phys. Chem. Chem. Phys.* **1999**, *1*, 1633.
(20) Mokaya, R.; Jones, W. *Phys. Chem. Chem. Phys.* **1999**, *1*, 207.
(21) Kustov, L. M.; Borovkov, V. Y.; Kazansky, V. B. *J. Catal.* **1981**, *72*, 149.
(22) Weckhuysen, B. M.; Schoofs, B.; Schoonheydt, R. A. *J. Chem. Soc., Faraday Trans.* **1997**, *93*, 2117.
(23) QPOW simulation program, Illinois EPR Research Center, at Urbana−Champaign.